Organic coating reduces hygroscopic growth of phase-separated aerosol particles

Li, Weijun; Teng, Xiaome; Chen, Xiyao; Liu, Lei; Xu, Liang; Zhang, Jian; Wang, Yuanyuan; Zhang, Yue; Shi, Zongbo

DOI:
10.1021/acs.est.1c05901

Document Version
Peer reviewed version

Citation for published version (Harvard):
Li, W, Teng, X, Chen, X, Liu, L, Xu, L, Zhang, J, Wang, Y, Zhang, Y & Shi, Z 2021, 'Organic coating reduces hygroscopic growth of phase-separated aerosol particles', *Environmental Science and Technology*, vol. 55, no. 24, pp. 16339-16346. https://doi.org/10.1021/acs.est.1c05901

Organic coating reduces hygroscopic growth of phase separated aerosol particles

Weijun Li[1*], Xiaome Teng[1], Xiyao Chen[1], Lei Liu[1], Liang Xu[1], Jian Zhang[1], Yuanyuan Wang[1], Yue Zhang[2], Zongbo Shi[3]

[1]Department of Atmospheric Sciences, School of Earth Sciences, Zhejiang University, Hangzhou, 310027, China

[2]Department of Atmospheric Sciences, Texas A&M University, College Station, TX, 77843, USA

[3]School of Geography, Earth and Environment Sciences, University of Birmingham, Birmingham B15 2TT, UK

*Corresponding Email: liweijun@zju.edu.cn (W. J. Li)

Abstract

A large fraction of secondary aerosol particles is liquid-liquid phase separation with organic shell and inorganic core. This has the potential to regulate the hygroscopicity of such particles, with significant implications for their optical properties, reactivity, and lifetime. However, it is unclear how this phase separation affects the hygroscopic growth of the particles. Here, we showed a large variation in hygroscopic growth (e.g., 1.14 -1.32 under RH 90%) of particles from forest and urban atmosphere, which had different average core-shell ratios. For this reason, a controlled laboratory experiment further quantify the impact of organic shell on particle growth with different RHs. Laboratory experiments demonstrated that $(NH_4)_2SO_4$ particles with thicker secondary organic shells have a lower growth factor at RH below 94%. Organic shells started to deliquesce first (RH>50%) and the phase changes of sulfate cores from solid to liquid took place at a RH larger than 80% as deliquescence relative humidity (DRH) of pure $(NH_4)_2SO_4$. Our study provides the first direct evidence on an individual particle basis that hygroscopic growth behavior of phase-separated particles is dependent on the thickness of organic shells, highlighting the importance of organic coating in water uptake and possible heterogeneous reactions of the phase-separated particles.

Keywords: Hygroscopicity, liquid-liquid phase separation, aerosol, particle phase

Synopsis: The study significantly extends our understanding of liquid-liquid phase-separated particles, how organic shell influences water uptake in the air, and constrains

hygroscopic growth of inorganic core.

Introduction

Atmospheric particles can directly or indirectly interact with sunlight and change the energy balance of Earth's atmosphere, with the water uptake process greatly altering the optical properties and the ability to act as cloud condensation nuclei (CCN) of these aerosol particles, thus influencing their climate properties.[1-3] In addition, the water uptake also influences the reactivity and lifetime of ambient particles, thereby affecting air quality and human health.[4, 5] For instance, condensed water provides a medium for the multiphase chemical reactions to happen within the particles[6, 7], which leads to changes in the gas uptake efficiency (e.g., N_2O_5 hydrolysis),[8-10] metal solubility,[11, 12] and the formation of secondary aerosol particles.[1, 13] Hygroscopicity is a key parameter to characterize the water uptake ability of aerosol particles.[2, 14, 15]

In the past decade, various advanced technologies have been used to investigate the hygroscopicity of aerosol particles collected both from the laboratory and the field campaign.[16] The hygroscopic tandem differential mobility analyzer (HTDMA) is one of the most commonly used techniques to investigate hygroscopic growth of aerosol particles under various environments.[17-19] Although the HTDMA significantly enhanced our understanding in the hygroscopicity of ambient aerosol particles, it provides an average growth factor (GF) of size-resolved aerosol populations.[1] Thus, it is unable to reveal the heterogeneity of the hygroscopicity within an aerosol population. Such heterogeneity often significantly impacts certain atmospheric processes, including the CCN activation of ambient particles.[2] To address this issue, a single particle technique has been used for hygroscopicity studies to understand the mixing state and

hygroscopicity of individual particles.[14, 20-24] These results[14, 20-24] show that individual ambient aerosol particles often exhibit as a mixture of inorganic sulfate, nitrate, and organic species of different ratios following the particle aging processes through different environments in the atmosphere. The large differences in the hygroscopicity of sulfate, nitrate, and organics,[14, 25] together with the composition differences of each individual particle, will likely lead to a wide range of growth factors of aerosol particles[26, 27] that needs to be considered in models for the formation, optical properties, and CCN activity of aerosol particles.[1, 2, 26]

Recently, the liquid-liquid phase separation of inorganic and organic components within a single particle has been examined as such effect can affect the water and gas uptake of the particles.[15, 28-30] Previous studies[20, 25, 28, 31, 32] confirmed that the core-shell phase-separation morphology widely exhibited in ambient particles through measurements performed by the transmission and scanning electron microscopy (TEM/SEM). However, the current studies analyzed the hygroscopicity of bulk collected samples under the typical air pollution events without examining the effects of phase separations.[19, 33, 34] Recent laboratory research on liquid-liquid phase separation showed that organic materials occurring as shells on the inorganic core of the particles are shown to have different impacts on early deliquescence of particle surface[15, 35, 36] as well as water and gas uptake (e.g., N_2O_5).[8, 9, 35] However, there is a lack of systematic study on the effects of organic shell (also called as organic coating) and inorganic core on hygroscopicity under different RH conditions. For instance, online instruments such as an aerosol time-of-flight mass spectrometer (ATOFMS) in

tandem to a HTDMA could observe mixing state and hygroscopicity of individual particles without providing the evidence of liquid-liquid phase separation.[1, 18, 23] Other studies on single particles often used a mixture of organic surrogates and inorganic species without further examining the effects of phase separations.[27, 28, 37-40] In addition, some studies reported the hygroscopic properties of the laboratory generated surrogate particles which are not consistent with the core-shell structure of the ambient particles.[27, 38] These results highlight the necessity to systematically examine how phase separation alters the hygroscopic properties of individual particles under different RHs using a single particle technique.

The aim of this study is to understand hygroscopic properties of liquid-liquid phase-separated particles. To achieve this aim, we first investigated the core-shell ratios and hygroscopic growth in airborne particles collected in different environmental air. We then found that the coating thickness might be a key factor affecting hygroscopic growth. To obtain direct evidence, we built a photochemical flow tube to produce organic aerosols to generate the internally mixed particles with ammonium sulfate core and organic shell. The thickness of the organic shells was controlled by changing the reaction time. Then an individual particle hygroscopic (IPH) system is constructed to continuously observe the hygroscopic growth processes of the phase-separated particles during 3-94% RH.

2. Experiments

2.1 Field campaigns

Aerosol particle samples were collected at three locations representing different

atmospheric environments: a forest site in the Lesser Khingan Mountains of northeastern China, urban Beijing of northern China, and urban Hangzhou of eastern China. Here we selected six typical samples which commonly include the core-shell particles for hygroscopic experiments. Table S1 shows meteorological data and sampling period of each sample. Aerosol samples are collected both onto copper TEM grids coated with carbon film and silicon wafers using a DKL-2 single particle sampler with a single-stage cascade impactor equipped with a 0.3 mm diameter jet nozzle at a flow of 1.0 liters per minute (lpm). The cutoff size of the impactor (50% collection efficiency) is 0.1 μm (aerodynamic diameter, assuming a material density of 2 g cm^{-3}). The collection time varied between 2-20 min, depending on the number concentrations of aerosol particles. After the aerosol collection, the samples were placed in sealed, dry, plastic capsules to prevent contamination. Then the samples were stored in a desiccator at 20 °C and 20 ± 3% RH for subsequent analysis.

2.2 TEM analysis

Imaging of the particles with cryo-TEM was conducted on a Talos F200C equipped with a Ceta 4k ×4k camera at the Center of Cryo-Electron Microscopy, Zhejiang University (Hangzhou, China), which is operated at 200 kV accelerating voltage. Samples were cooled in the cryo-TEM to approximately 104 K using a liquid nitrogen cooling cryo-TEM holder before exposure to electron radiation to reduce damage to the particles. The cryo-TEM is one efficient way to observe the original state of individual secondary particles on the substrate because the secondary nitrates or sulfates receive minimum damage from the electron radiation when the images are taken. To further

confirm composition and mixing state of individual ambient particles collected on TEM grids, a JEOL JEM-2100 transmission electron microscope operated at 200 kV with energy-dispersive X-ray spectrometry (TEM/EDX) was conducted. The scanning TEM (STEM) function was adopted to obtain line scanning of elemental composition on individual particles which can directly reflect different aerosol components to form the core-shell structure. Finally, these microscopic observations are used to explain hygroscopic behaviors of individual aerosol particles.

2.3 Hygroscopic experiment

In this study, an individual particle hygroscopicity (IPH) system was built to investigate the hygroscopic properties of individual particles at different RHs. The experimental process is composed of three steps: (1) Introducing N_2 gas with controlled flow by a mass flow controller into a chamber; (2) Mounting the TEM grid or silicon wafer with particles on the bottom of an environmental microscopic cell (Gen-RH Mcell, UK), which can change RH while maintaining a constant temperature of 20 ± 1 ^{o}C; (3) Taking images at different RH through an optical microscope (Olympus BX51M, Japan) with a camera (Canon 650D). A similar experimental set-up is described elsewhere.[26, 41] (4) The equivalent circle diameter of each individual particle in images were analyzed using image analysis software (Radius, EMSIS GmbH, Germany). We manually obtained sizes of the same particle at different RHs and further calculated its GF.

The pure $(NH_4)_2SO_4$ particles with the size range of 0.5-20 μm was made in laboratory and collected on silicon wafer substrates and TEM grids. Hygroscopic

147 behaviors of these $(NH_4)_2SO_4$ particles were used to test the IPH system at different
148 RHs from 3% to 94%. The deliquescence relative humidity (DRH) of all particles were
149 observed to be 80±2 %, which is consistent with the theoretical DRH of $(NH_4)_2SO_4$
150 (Figure S2). Following the control study, nine laboratory-generated samples and six
151 samples collected in the ambient air were chosen to observe particle hygroscopic
152 growth in the IPH system. The images taken by the IPH system were used to compare
153 their morphology and size at different RH values (e.g., Figure S2). Particle GF from
154 this study is calculated using Eqn. 1 below.

155 $$GF\,(RH) = \frac{D(RH)}{D_0} \qquad (1)$$

156 Where *D(RH)* is the diameter of particles at a given RH, D_0 is the diameter of dry
157 particles at 5% RH. The GF curve of individual particles can be used to understand
158 changes of particle phase and size growth under different RHs.[26] Finally, we tried to
159 select 5-8 core-shell particles of each sample in the optical images and calculated their
160 average GF.

161 **2.4 Laboratory experiment**

162 Individual $(NH_4)_2SO_4$ particles on silicon wafers and TEM grids are prepared
163 following the procedure reported by Sun et al. (2018).[26] After leaving the $(NH_4)_2SO_4$
164 sample in an enclosed container for two hours to allow equilibrium with the
165 environment, the prepared samples are placed at the outflow tip of the flow tube. Figure
166 S1 shows the flow tube including three main parts: the gas inlet, the reaction tube, and
167 the outlet. The similar flow tube was tested and widely used to study secondary aerosol
168 formation in the laboratory experiment.[42] In this study, 0.1 lpm of air was used to

vaporize liquid α-pinene while 1.5 lpm of pure nitrogen and 1.5 lpm O_3 were mixed within a 2-liter glass tube with UV-B lights on to react and produce the secondary organic materials that can be coated onto the existing $(NH_4)_2SO_4$ particles. The organic materials from oxidizing α-pinene are observed to form a layer of film on the substrate as the control experiment. All the samples contain individual particles with organic shell and sulfate core on the substrate after the 11h, 15h, and 20h of secondary organic materials exposure in the flow tube, which is used to produce organic shell with different thickness in different periods. Upon the flow tube experiments, the samples were conditioned at three hygroscopic cycles ramping from 3-94% RH in the IPH. During the hygroscopic growth of individual particles, the organic matter surrounding the inorganic sulfate core always maintained its stable organic shell on individual particles. In total, three parallel experiments of each with six silicon wafers samples are collected for hygroscopic experiments and nine TEM grids are collected for chemical analysis.

3 Results and Discussion

3.1 Phase separation of organic and sulfate in secondary aerosols

Cryo-TEM and TEM observations both revealed a common core–shell mixing structure (i.e., liquid-liquid phase separation) in the aerosol particles collected in different environmental conditions, as shown in Figures 1 and S3. EDS shows that the core part mainly contains S, O, N elements and the shell part is dominant by the C and minor O elements (Figure S3). Figure 1a-b also clearly shows various intact secondary organic-inorganic phase separated particles that were collected from ambient

191 environments. The line scanning in STEM shows that the core exhibits high
192 concentration of O and S and the shell exhibits more C. Based on the distribution of
193 elemental composition and mixing state of individual particles, we can conclude that
194 the cores of these ambient particles are dominated by inorganic sulfates/nitrates and the
195 shells mainly contain secondary organic matter, agreeing with the liquid-liquid phase
196 separation reported in previous studies.[15, 20, 25]

197 In this study, we found that over 59% of secondary inorganic aerosols have the
198 organic shells in background forest particles and 36-45% in the urban particles in
199 summer (Table S1). Recently, Yu et al., (2019)[31] revealed that 74% of secondary
200 inorganic aerosols have thick organic shell in remote Arctic air. These results suggest
201 that a large portion of the secondary aerosol particles is phase-separated under ambient
202 conditions. This phase separation has the potential to impact water uptake of inorganic
203 cores at selected RH levels and thus influencing the heterogeneous reactions and CCN
204 activities of individual particles.[2, 8, 19]

205 **3.2 Hygroscopic behavior of ambient phase-separated particles**

206 Figure 2a lists the optical image of ambient particles collected from ambient
207 environment, showing that organic shells in individual secondary particles all start to
208 grow up at RH=50% in all the samples, whether from the forest or urban air. As the RH
209 increases, the particles collected in forest air grow continuously and then are converted
210 into liquid phase when the RH reaches 84% (Figure S4). For particles collected under
211 the urban environment, the continuous growth of the inorganic cores and organic shells
212 become liquid phase at 83% RH (Figure 2a and Figures S5-6). We noticed that the urban

aerosol particles have more abrupt hygroscopic growth above RH=60% compared with the forest aerosol particles. Given that Sun et al., (2018)[26] found that phase of secondary aerosol particles start changes at 60±1% RH due to the presence of ammonium nitrate and the wide presence of inorganic nitrate in urban aerosols,[20] it is likely that these analyzed particles also contain inorganic nitrate. The presence of ammonium nitrate in individual particles might slightly enhance GF of individual urban particles at 60-80% RH, as shown in Figure 2a.

Figure 2a shows the average GFs of aerosol particles at RH=90%: ~1.14 in forest environment, 1.21-1.32 in urban environments, indicating the GF of secondary aerosol particles collected in forest environment is much lower than those in the urban environment. Moreover, the GFs of urban aerosol particles are much lower than that of the pure ammonium nitrate and ammonium sulfate particles (1.61-1.75) measured by the IPH techniques.[26] We noticed that the average thicknesses of organic shells in the core-shell particles collected in Beijing, Hangzhou, and lesser Khingan mountain air were 60 nm, 86 nm, and 110 nm, respectively (Table S1). Therefore, we hypothesize that the organic shells contribute to the lowering of GFs among different liquid-liquid phase separation particles.

This hypothesis cannot be tested in airborne particles because it is not feasible to characterize the same individual particles with both IPH and TEM, which provide growth and shell thickness separately. For this reason, a controlled laboratory experiment was carried out to systematically quantify the impact of organic shell on particle growth with different RHs (see below).

3.3 Hygroscopic effects of laboratory generated phase-separated organic-inorganic particles

To achieve the above aim, we prepared laboratory generated liquid-liquid phase separation particles with different thickness of organic shells through a flow tube (Figure S1). TEM observation confirmed that the laboratory generated particles clearly displayed a typical organic shell and sulfate core structure (Figure 3). Figure 4 shows similar shell thickness among different particles in the optical images of laboratory generated particles (11 hours aging) exposed to RH ranging from 3-94%. Organic shell started to uptake water and increased its thickness at 50% RH but never fully deliquesced while the sulfate cores did not grow until 81% RH. The core then gradually changed from solid to liquid phase (Figure 2b) at 83%, which is different and higher than the abrupt phase change at 81% for the pure $(NH_4)_2SO_4$. This indicates that the hygroscopic growth of sulfate cores was inhibited by the secondary organic shells.

Two additional experiments were carried out to investigate whether the thickness of the organic shell may affect the hygroscopic growth behavior of ammonium sulfate. Figures 2b (green line) and S7 show that phase separated particles (15 h of exposure in the flow tube) started to change at 50% and sulfate cores started to grow at 81% but did not completely deliquesce until 84.5% RH. Figures 2b and S8 show that phase separated particles (21 h of exposure in the flow tube) started to change at 50% RH and sulfate cores grew at 86% RH but did not completely deliquesce until at 90% RH. In addition, the small error bars show that the GFs among different particles have similar values (Figure 2b), suggesting that the laboratory-generated particles display similar

hygroscopic properties in the same sample. Therefore, we can conclude that the increasing thickness of the organic shells (Figures 2b and S7-8) raised the DRH of the sulfate cores.

The optical images show that individual particles clearly demonstrated different deliquescence changes regarding the core and shell, contrary to the results reported in previous bulk-measured studies that observed changes of the whole particles as a function of RHs.[1, 27, 43] This difference could be explained by the inherent inaccuracy in the aerosol population, which does not account for the thickness of organic shell and mixing state, e.g., using the HTDMA.

We repeated the three RH cycles for each sample at the range of 3-94% RH and observed the same GFs each time, while the GFs of individual particles decrease as the time of exposure increases in the flow tube. For instance, Figure 2b shows that individual particles exposed for 11, 15, and 21 hrs in the flow tube displayed GFs at 1.5, 1.4, and 1.2 under the RH=90%, respectively, suggesting that thicker organic shells suppress the GF of the individual particles. The GF values of the phase separated particles varied between the 1.07-1.67,[44] with the upper value equal to the GF of the pure $(NH_4)_2SO_4$ (e.g., 1.67 at RH=85% shown in Figure 2b). Moreover, the inorganic sulfate cores show a slower growth curve as the shell thickness of the organic shells increase (Figure 2b), when comparing with an abrupt phase change of the pure $(NH_4)_2SO_4$ at DRH=81%. Nevertheless, Figures 2 and 4 show that hygroscopic growth is mainly associated with the deliquescence of the sulfate cores while the organic shell has limited influence. The above result indicates that secondary organic shells

279 significantly affect the deliquescence and growth of the inorganic particles. The organic
280 shell suppresses the water uptake of sulfate cores, that is, limiting the water diffusion
281 to the particle core.

282 Once the particles deliquesced following water uptake, they might keep water in
283 the particles until 43% RH during the dehydration. The reason is that sulfate cores in
284 the phase-separated particles effloresced from liquid to solid phase until the RH down
285 to 41-43%, which is lower than the efflorescence relative humidity at 48% of the pure
286 ammonium sulfate (Figures S9-S10). In other words, the organic shells can limit water
287 evaporation from the sulfate cores.

288 In summary, our study confirmed the hypothesis that the thickness of the organic
289 shells contributes to the lowering of GFs among different liquid-liquid phase separation
290 particles. We recognize that chemical composition of the coating also has the potential
291 to affect the hygroscopic growth. This should be investigated further in future field and
292 laboratory experiments.

293 **3.4 Summary and atmospheric implications**

294 The synthetic experiment demonstrated that organic shells in the ambient liquid-
295 liquid phase separation particles, commonly present in forest and urban environments,
296 act as barriers for the water vapor exchange to the inorganic cores. This also indicates
297 that organic coating reduces the mass accommodation coefficient for gases (e.g., N_2O_5)
298 at surfaces[10], leading to a reduction of the formation of secondary organic aerosols.[45]
299 The presence of organic species at the particle surface also influences the CCN
300 activation by altering the surface tension and the water activity, leading to changes in

301 the equilibrium vapor pressure of water over these solution droplets.[2, 29, 46, 47]

302 Previous studies also showed that organic shells can be semi-solid with high
303 viscosity,[45, 48, 49] leading to slower heterogeneous reaction rates. The very small growth
304 factor of the laboratory particles at 50-80% (Figure 2) implies that the organic shells
305 are semi-solid (T=295 K), consistent with reported viscosity of secondary organic
306 aerosols in field and laboratory experiments.[50-53] Once the organic shell becomes
307 aqueous phase at above 50% RH, the wet organic shell may further influence the
308 formation of sulfate and nitrate in the aqueous phase (aqSOA) from photo-oxidation.[54,
309 55] Information regarding phase-separated particles should be incorporated into the
310 atmospheric modeling for heterogeneous chemistry as well as particle hygroscopicity
311 and growth to improve predictions on air quality and indirect effects of aerosol-climate
312 interactions.

ASSOCIATED CONTENT

Supporting information

Detailed description of hygroscopic growth and data analysis (Table S1 and Figure S1-S8)

AUTHOR INFORMATION

Corresponding authors

Weijun Li-Department of Atmospheric Sciences, School of Earth Sciences, Zhejiang University, 310027, Hangzhou, China

Authors

Xiaome Teng-Department of Atmospheric Sciences, School of Earth Sciences, Zhejiang University, 310027, Hangzhou, China

Xiyao Chen-Department of Atmospheric Sciences, School of Earth Sciences, Zhejiang University, 310027, Hangzhou, China

Lei Liu-Department of Atmospheric Sciences, School of Earth Sciences, Zhejiang University, 310027, Hangzhou, China

Liang Xu-Department of Atmospheric Sciences, School of Earth Sciences, Zhejiang University, 310027, Hangzhou, China

Jian Zhang-Department of Atmospheric Sciences, School of Earth Sciences, Zhejiang University, 310027, Hangzhou, China

Yuanyuan Wang-Department of Atmospheric Sciences, School of Earth Sciences, Zhejiang University, 310027, Hangzhou, China

Yue Zhang-Department of Atmospheric Sciences, Texas A&M University, College Station, TX, 77843, USA

Zongbo Shi-School of Geography, Earth and Environment Sciences, University of Birmingham, Birmingham B15 2TT, UK

Notes

The authors declare no competing financial interest.

Acknowledgments Cryo-EM characterization was conducted at the Center of Cryo-Electron Microscopy, Zhejiang University, with the assistance of L. Wu. We gratefully acknowledge Shujia Zhang to conduct part of the laboratory experiments. The work was funded by the National Natural Science Foundation of China (91844301 and 42075096), Zhejiang Provincial Natural Science Foundation of China (LZ19D050001).

All the data are presented in the paper.

References:

[1] Wang, X.; Ye, X.; Chen, J.; Wang, X.; Yang, X.; Fu, T. M.; Zhu, L.; Liu, C. Direct links between hygroscopicity and mixing state of ambient aerosols: estimating particle hygroscopicity from their single-particle mass spectra. *Atmos. Chem. Phys.* **2020,** *20*, (11), 6273-6290.

[2] Farmer, D. K.; Cappa, C. D.; Kreidenweis, S. M. Atmospheric Processes and Their Controlling Influence on Cloud Condensation Nuclei Activity. *Chem. Rev.* **2015,** *115*, (10), 4199-4217.

[3] Li, K.; Li, J.; Wang, W.; Li, J.; Peng, C.; Wang, D.; Ge, M. Effects of Gas-Particle Partitioning on Refractive Index and Chemical Composition of m-Xylene Secondary Organic Aerosol. *J. Phys. Chem. A.* **2018,** *122*, (12), 3250-3260.

[4] Hodas, N.; Sullivan, A. P.; Skog, K.; Keutsch, F. N.; Collett, J. L.; Decesari, S.; Facchini, M. C.; Carlton, A. G.; Laaksonen, A.; Turpin, B. J. Aerosol liquid water driven by anthropogenic nitrate: implications for lifetimes of water-soluble organic gases and potential for secondary organic aerosol formation. *Environ. Sci. Technol.* . **2014,** *48*, (19), 11127-11136.

[5] Ervens, B. Modeling the pocessing of aerosol and trace gases in clouds and fogs. *Chem. Rev.* **2015,** *115*, (10), 4157-4198.

[6] Herrmann, H.; Schaefer, T.; Tilgner, A.; Styler, S. A.; Weller, C.; Teich, M.; Otto, T. Tropospheric Aqueous-Phase Chemistry: Kinetics, Mechanisms, and Its Coupling to a Changing Gas Phase. *Chem. Rev.* **2015,** *115*, (10), 4259-4334.

[7] Wang, W.; Liu, M.; Wang, T.; Song, Y.; Zhou, L.; Cao, J.; Hu, J.; Tang, G.; Chen, Z.; Li, Z.; Xu, Z.; Peng, C.; Lian, C.; Chen, Y.; Pan, Y.; Zhang, Y.; Sun, Y.; Li, W.; Zhu, T.; Tian, H.; Ge, M. Sulfate formation is dominated by manganese-catalyzed oxidation of SO2 on aerosol surfaces during haze events. *Nat. Commun.* **2021,** *12*, (1), 1993.

[8] Wang, H.; Chen, X.; Lu, K.; Tan, Z.; Ma, X.; Wu, Z.; Li, X.; Liu, Y.; Shang, D.; Wu, Y.; Zeng, L.; Hu, M.; Schmitt, S.; Kiendler-Scharr, A.; Wahner, A.; Zhang, Y. Wintertime N2O5 uptake coefficients over the North China Plain. *Sci Bull.* **2020,** *65*, (9), 765-774.

[9] Liu, J.; Li, S.; Mekic, M.; Jiang, H.; Zhou, W.; Loisel, G.; Song, W.; Wang, X.; Gligorovski, S. Photoenhanced Uptake of NO2 and HONO Formation on Real Urban Grime. *Environ. Sci. Techn. Lett.* **2019,** *6*, (7), 413-417.

[10] Badger, C. L.; Griffiths, P. T.; George, I.; Abbatt, J. P. D.; Cox, R. A. Reactive Uptake of N2O5 by Aerosol Particles Containing Mixtures of Humic Acid and Ammonium Sulfate. *J. Phys. Chem. A.* **2006,** *110*, (21), 6986-6994.

[11] Zhu, Y.; Li, W.; Lin, Q.; Yuan, Q.; Liu, L.; Zhang, J.; Zhang, Y.; Shao, L.; Niu, H.; Yang, S.; Shi, Z. Iron solubility in fine particles associated with secondary acidic aerosols in east China. *Environ. Pollut.* **2020,** *264*, 114769.

[12] Li, W.; Xu, L.; Liu, X.; Zhang, J.; Lin, Y.; Yao, X.; Gao, H.; Zhang, D.; Chen, J.; Wang, W.; Harrison, R. M.; Zhang, X.; Shao, L.; Fu, P.; Nenes, A.; Shi, Z. Air pollution–aerosol interactions produce more bioavailable iron for ocean ecosystems. *Sci. Adv.* **2017,** *3*, (3), e1601749, 1-6.

[13] Wu, Z.; Wang, Y.; Tan, T.; Zhu, Y.; Li, M.; Shang, D.; Wang, H.; Lu, K.; Guo, S.; Zeng, L.; Zhang, Y. Aerosol Liquid Water Driven by Anthropogenic Inorganic Salts: Implying Its Key Role in Haze Formation over the North China Plain. *Environ. Sci. Techn. Lett.* **2018,** *5*, (3), 160-166.

[14] Riemer, N.; Ault, A. P.; West, M.; Craig, R. L.; Curtis, J. H. Aerosol Mixing State: Measurements, Modeling, and Impacts. *Rev. Geophys.* **2019,** *57*, https://doi.org/10.1029/2018RG000615.

[15] You, Y.; Renbaum-Wolff, L.; Carreras-Sospedra, M.; Hanna, S. J.; Hiranuma, N.; Kamal, S.; Smith, M. L.; Zhang, X.; Weber, R. J.; Shilling, J. E.; Dabdub, D.; Martin, S. T.; Bertram, A. K. Images reveal

that atmospheric particles can undergo liquid–liquid phase separations. *P. Natl. Acad. Sci. USA.* **2012,** *109*, (33), 13188-13193.
[16] Tang, M.; Chan, C. K.; Li, Y. J.; Su, H.; Ma, Q.; Wu, Z.; Zhang, G.; Wang, Z.; Ge, M.; Hu, M.; He, H.; Wang, X. A review of experimental techniques for aerosol hygroscopicity studies. *Atmos. Chem. Phys.* **2019,** *19*, (19), 12631-12686.
[17] Swietlicki, E.; Hansson, H. C.; Hameri, K.; Svenningsson, B.; Massling, A.; McFiggans, G.; McMurry, P. H.; Petaja, T.; Tunved, P.; Gysel, M.; Topping, D.; Weingartner, E.; Baltensperger, U.; Rissler, J.; Wiedensohler, A.; Kulmala, M. Hygroscopic properties of submicrometer atmospheric aerosol particles measured with H-TDMA instruments in various environments - a review. *Tellus B.* **2008,** *60*, (3), 432-469.
[18] Kuang, Y.; Zhao, C. S.; Ma, N.; Liu, H. J.; Bian, Y. X.; Tao, J. C.; Hu, M. Deliquescent phenomena of ambient aerosols on the North China Plain. *Geophy. Res. Lett.* **2016,** *43*, (16), 8744-8750.
[19] Pajunoja, A.; Hu, W.; Leong, Y. J.; Taylor, N. F.; Miettinen, P.; Palm, B. B.; Mikkonen, S.; Collins, D. R.; Jimenez, J. L.; Virtanen, A. Phase state of ambient aerosol linked with water uptake and chemical aging in the southeastern US. *Atmos. Chem. Phys.* **2016,** *16*, (17), 11163-11176.
[20] Li, W.; Sun, J.; Xu, L.; Shi, Z.; Riemer, N.; Sun, Y.; Fu, P.; Zhang, J.; Lin, Y.; Wang, X.; Shao, L.; Chen, J.; Zhang, X.; Wang, Z.; Wang, W. A conceptual framework for mixing structures in individual aerosol particles. *J. Geophys. Res.* **2016,** *121*, (22), 13,784-13,798.
[21] Laskin, A.; Moffet, R. C.; Gilles, M. K. Chemical Imaging of Atmospheric Particles. *Accounts Chem. Res.* **2019,** *52*, (12), 3419-3431.
[22] Olson, N.; Xiao, Y.; Lei, Z.; Ault, A. Simultaneous Optical Photothermal Infrared (O-PTIR) and Raman Spectroscopy of Submicrometer Atmospheric Particles. *Microsc. Microanal.* **2020,** *26*, (S2), 2752-2753.
[23] Ault, A. P.; Axson, J. L. Atmospheric Aerosol Chemistry: Spectroscopic and Microscopic Advances. *Anal. Chem.* **2017,** *89*, (1), 430-452.
[24] Zhang, G.; Lin, Q.; Peng, L.; Bi, X.; Chen, D.; Li, M.; Li, L.; Brechtel, F. J.; Chen, J.; Yan, W.; Wang, X.; Peng, P.; Sheng, G.; Zhou, Z. The single-particle mixing state and cloud scavenging of black carbon: a case study at a high-altitude mountain site in southern China. *Atmos. Chem. Phys.* **2017,** *17*, (24), 14975-14985.
[25] Li, W.; Liu, L.; Zhang, J.; Xu, L.; Wang, Y.; Sun, Y.; Shi, Z. Microscopic Evidence for Phase Separation of Organic Species and Inorganic Salts in Fine Ambient Aerosol Particles. *Environ. Sci. Techn.* **2021,** *55*, (4), 2234-2242.
[26] Sun, J.; Liu, L.; Xu, L.; Wang, Y.; Wu, Z.; Hu, M.; Shi, Z.; Li, Y.; Zhang, X.; Chen, J.; Li, W. Key Role of Nitrate in Phase Transitions of Urban Particles: Implications of Important Reactive Surfaces for Secondary Aerosol Formation. *J. Geophy. Res.* **2018,** *123*, (2), 1234-1243.
[27] Jing, B.; Wang, Z.; Tan, F.; Guo, Y.; Tong, S.; Wang, W.; Zhang, Y.; Ge, M. Hygroscopic behavior of atmospheric aerosols containing nitrate salts and water-soluble organic acids. *Atmos. Chem. Phys.* **2018,** *18*, (7), 5115-5127.
[28] O'Brien, R. E.; Wang, B.; Kelly, S. T.; Lundt, N.; You, Y.; Bertram, A. K.; Leone, S. R.; Laskin, A.; Gilles, M. K. Liquid–Liquid Phase Separation in Aerosol Particles: Imaging at the Nanometer Scale. *Environ. Sci. Techn.* **2015,** *49*, (8), 4995-5002.
[29] Pye, H. O. T.; Murphy, B. N.; Xu, L.; Ng, N. L.; Carlton, A. G.; Guo, H.; Weber, R.; Vasilakos, P.; Appel, K. W.; Budisulistiorini, S. H.; Surratt, J. D.; Nenes, A.; Hu, W.; Jimenez, J. L.; Isaacman-VanWertz, G.; Misztal, P. K.; Goldstein, A. H. On the implications of aerosol liquid water and phase

separation for organic aerosol mass. *Atmos. Chem. Phys.* **2017,** *17*, (1), 343-369.
[30] Freedman, M. A. Liquid–Liquid Phase Separation in Supermicrometer and Submicrometer Aerosol Particles. *Accounts Chem. Res.* **2020,** *53*, (6), 1102-1110.
[31] Yu, H.; Li, W.; Zhang, Y.; Tunved, P.; Dall'Osto, M.; Shen, X.; Sun, J.; Zhang, X.; Zhang, J.; Shi, Z. Organic coating on sulfate and soot particles during late summer in the Svalbard Archipelago. *Atmos. Chem. Phys.* **2019,** *19*, (15), 10433-10446.
[32] Adachi, K.; Buseck, P. R. Internally mixed soot, sulfates, and organic matter in aerosol particles from Mexico City. *Atmos. Chem. Phys.* **2008,** *8*, (21), 6469-6481.
[33] Chen, J.; Budisulistiorini, S. H.; Miyakawa, T.; Komazaki, Y.; Kuwata, M. Secondary aerosol formation promotes water uptake by organic-rich wildfire haze particles in equatorial Asia. *Atmos. Chem. Phys.* **2018,** *18*, (11), 7781-7798.
[34] Shingler, T.; Sorooshian, A.; Ortega, A.; Crosbie, E.; Wonaschütz, A.; Perring, A. E.; Beyersdorf, A.; Ziemba, L.; Jimenez, J. L.; Campuzano-Jost, P.; Mikoviny, T.; Wisthaler, A.; Russell, L. M. Ambient observations of hygroscopic growth factor and f(RH) below 1: Case studies from surface and airborne measurements. *J. Geophy. Res.* **2016,** *121*, (22), 13,661-13,677.
[35] Ruehl, C. R.; Wilson, K. R. Surface Organic Monolayers Control the Hygroscopic Growth of Submicrometer Particles at High Relative Humidity. *J. Phys. Chem. A.* **2014,** *118*, (22), 3952-3966.
[36] Kuai, Y.; Xie, Z.; Chen, J.; Gui, H.; Xu, L.; Kuang, C.; Wang, P.; Liu, X.; Liu, J.; Lakowicz, J. R.; Zhang, D. Real-Time Measurement of the Hygroscopic Growth Dynamics of Single Aerosol Nanoparticles with Bloch Surface Wave Microscopy. *ACS Nano.* **2020,** *14*, (7), 9136-9144.
[37] Estillore, A. D.; Morris, H. S.; Or, V. W.; Lee, H. D.; Alves, M. R.; Marciano, M. A.; Laskina, O.; Qin, Z.; Tivanski, A. V.; Grassian, V. H. Linking hygroscopicity and the surface microstructure of model inorganic salts, simple and complex carbohydrates, and authentic sea spray aerosol particles. *Phys. Chem. Chem. Phys.* **2017,** *19*, (31), 21101-21111.
[38] Li, X.; Gupta, D.; Lee, J.; Park, G.; Ro, C.-U. Real-Time Investigation of Chemical Compositions and Hygroscopic Properties of Aerosols Generated from NaCl and Malonic Acid Mixture Solutions Using in Situ Raman Microspectrometry. *Environ. Sci. Techn.* **2017,** *51*, (1), 263-270.
[39] Marcolli, C.; Krieger, U. K. Phase Changes during Hygroscopic Cycles of Mixed Organic/Inorganic Model Systems of Tropospheric Aerosols. *J. Phys. Chem. A.* **2006,** *110*, (5), 1881-1893.
[40] Chan, M. N.; Lee, A. K. Y.; Chan, C. K. Responses of Ammonium Sulfate Particles Coated with Glutaric Acid to Cyclic Changes in Relative Humidity: Hygroscopicity and Raman Characterization. *Environ. Sci. Techn.* **2006,** *40*, (22), 6983-6989.
[41] Ahn, K. H.; Kim, S. M.; Jung, H. J.; Lee, M. J.; Eom, H. J.; Maskey, S.; Ro, C. U. Combined use of optical and electron microscopic techniques for the measurement of hygroscopic property, chemical composition, and morphology of individual aerosol particles. *Anal. Chem.* **2010,** *82*, (19), 7999-8009.
[42] Huang, Y.; Coggon, M. M.; Zhao, R.; Lignell, H.; Bauer, M. U.; Flagan, R. C.; Seinfeld, J. H. The Caltech Photooxidation Flow Tube reactor: design, fluid dynamics and characterization. *Atmos. Meas. Tech.* **2017,** *10*, (3), 839-867.
[43] Zawadowicz, M. A.; Proud, S. R.; Seppalainen, S. S.; Cziczo, D. J. Hygroscopic and phase separation properties of ammonium sulfate/organics/water ternary solutions. *Atmos. Chem. Phys.* **2015,** *15*, (15), 8975-8986.
[44] Pajunoja, A.; Lambe, A. T.; Hakala, J.; Rastak, N.; Cummings, M. J.; Brogan, J. F.; Hao, L.; Paramonov, M.; Hong, J.; Prisle, N. L.; Malila, J.; Romakkaniemi, S.; Lehtinen, K. E. J.; Laaksonen, A.; Kulmala, M.; Massoli, P.; Onasch, T. B.; Donahue, N. M.; Riipinen, I.; Davidovits, P.; Worsnop, D. R.;

Petäjä, T.; Virtanen, A. Adsorptive uptake of water by semisolid secondary organic aerosols. *Geophy. Res. Lett.* **2015,** *42*, (8), 2015GL063142.
[45] Zhang, Y.; Chen, Y.; Lambe, A. T.; Olson, N. E.; Lei, Z.; Craig, R. L.; Zhang, Z.; Gold, A.; Onasch, T. B.; Jayne, J. T.; Worsnop, D. R.; Gaston, C. J.; Thornton, J. A.; Vizuete, W.; Ault, A. P.; Surratt, J. D. Effect of the Aerosol-Phase State on Secondary Organic Aerosol Formation from the Reactive Uptake of Isoprene-Derived Epoxydiols (IEPOX). *Environ. Sci. Techn. Lett.* **2018,** *5*, (3), 167-174.
[46] Werner, J.; Dalirian, M.; Walz, M.-M.; Ekholm, V.; Wideqvist, U.; Lowe, S. J.; Öhrwall, G.; Persson, I.; Riipinen, I.; Björneholm, O. Surface Partitioning in Organic–Inorganic Mixtures Contributes to the Size-Dependence of the Phase-State of Atmospheric Nanoparticles. *Environ. Sci. Techn.* **2016,** *50*, (14), 7434-7442.
[47] Davies, J. F.; Miles, R. E. H.; Haddrell, A. E.; Reid, J. P. Influence of organic films on the evaporation and condensation of water in aerosol. *P. Natl. Acad. Sci. USA.* **2013,** *110*, (22), 8807-8812.
[48] Zhang, Y.; Chen, Y.; Lei, Z.; Olson, N. E.; Riva, M.; Koss, A. R.; Zhang, Z.; Gold, A.; Jayne, J. T.; Worsnop, D. R.; Onasch, T. B.; Kroll, J. H.; Turpin, B. J.; Ault, A. P.; Surratt, J. D. Joint Impacts of Acidity and Viscosity on the Formation of Secondary Organic Aerosol from Isoprene Epoxydiols (IEPOX) in Phase Separated Particles. *ACS Earth and Space Chem.* **2019,** *3*, (12), 2646-2658.
[49] Saukko, E.; Zorn, S.; Kuwata, M.; Keskinen, J.; Virtanen, A. Phase State and Deliquescence Hysteresis of Ammonium-Sulfate-Seeded Secondary Organic Aerosol. *Aerosol Sci. Tech.* **2015,** *49*, (7), 531-537.
[50] Reid, J. P.; Bertram, A. K.; Topping, D. O.; Laskin, A.; Martin, S. T.; Petters, M. D.; Pope, F. D.; Rovelli, G. The viscosity of atmospherically relevant organic particles. *Nat. Commun.* **2018,** *9*, (1), 956.
[51] Renbaum-Wolff, L.; Grayson, J. W.; Bateman, A. P.; Kuwata, M.; Sellier, M.; Murray, B. J.; Shilling, J. E.; Martin, S. T.; Bertram, A. K. Viscosity of α-pinene secondary organic material and implications for particle growth and reactivity. *P. Natl. Acad. Sci. USA.* **2013,** *110*, (20), 8014-8019.
[52] Liu, P.; Song, M.; Zhao, T.; Gunthe, S. S.; Ham, S.; He, Y.; Qin, Y. M.; Gong, Z.; Amorim, J. C.; Bertram, A. K.; Martin, S. T. Resolving the mechanisms of hygroscopic growth and cloud condensation nuclei activity for organic particulate matter. *Nat. Commun.* **2018,** *9*, (1), 4076.
[53] Wang, Y.; Voliotis, A.; Shao, Y.; Zong, T.; Meng, X.; Du, M.; Hu, D.; Chen, Y.; Wu, Z.; Alfarra, M. R.; McFiggans, G. Phase state of secondary organic aerosol in chamber photo-oxidation of mixed precursors. *Atmos. Chem. Phys.* **2021,** *21*, (14), 11303-11316.
[54] Wang, Y.; Mekic, M.; Li, P.; Deng, H.; Liu, S.; Jiang, B.; Jin, B.; Vione, D.; Gligorovski, S. Ionic Strength Effect Triggers Brown Carbon Formation through Heterogeneous Ozone Processing of Ortho-Vanillin. *Environ. Sci. Techn.* **2021,** *55*, (8), 4553-4564.
[55] Huang, D. D.; Zhang, Q.; Cheung, H. H. Y.; Yu, L.; Zhou, S.; Anastasio, C.; Smith, J. D.; Chan, C. K. Formation and Evolution of aqSOA from Aqueous-Phase Reactions of Phenolic Carbonyls: Comparison between Ammonium Sulfate and Ammonium Nitrate Solutions. *Environ. Sci. Techn.* **2018,** *52*, (16), 9215-9224.

519 Abstract Graph

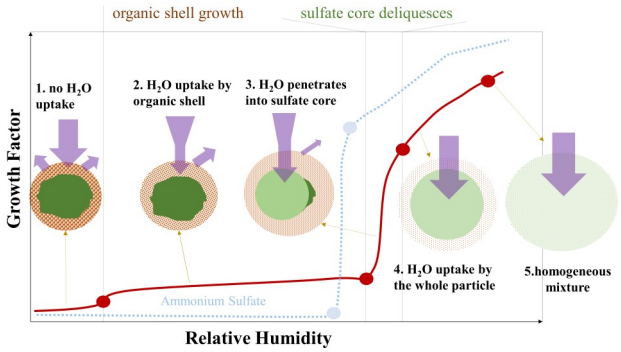

520

521

522

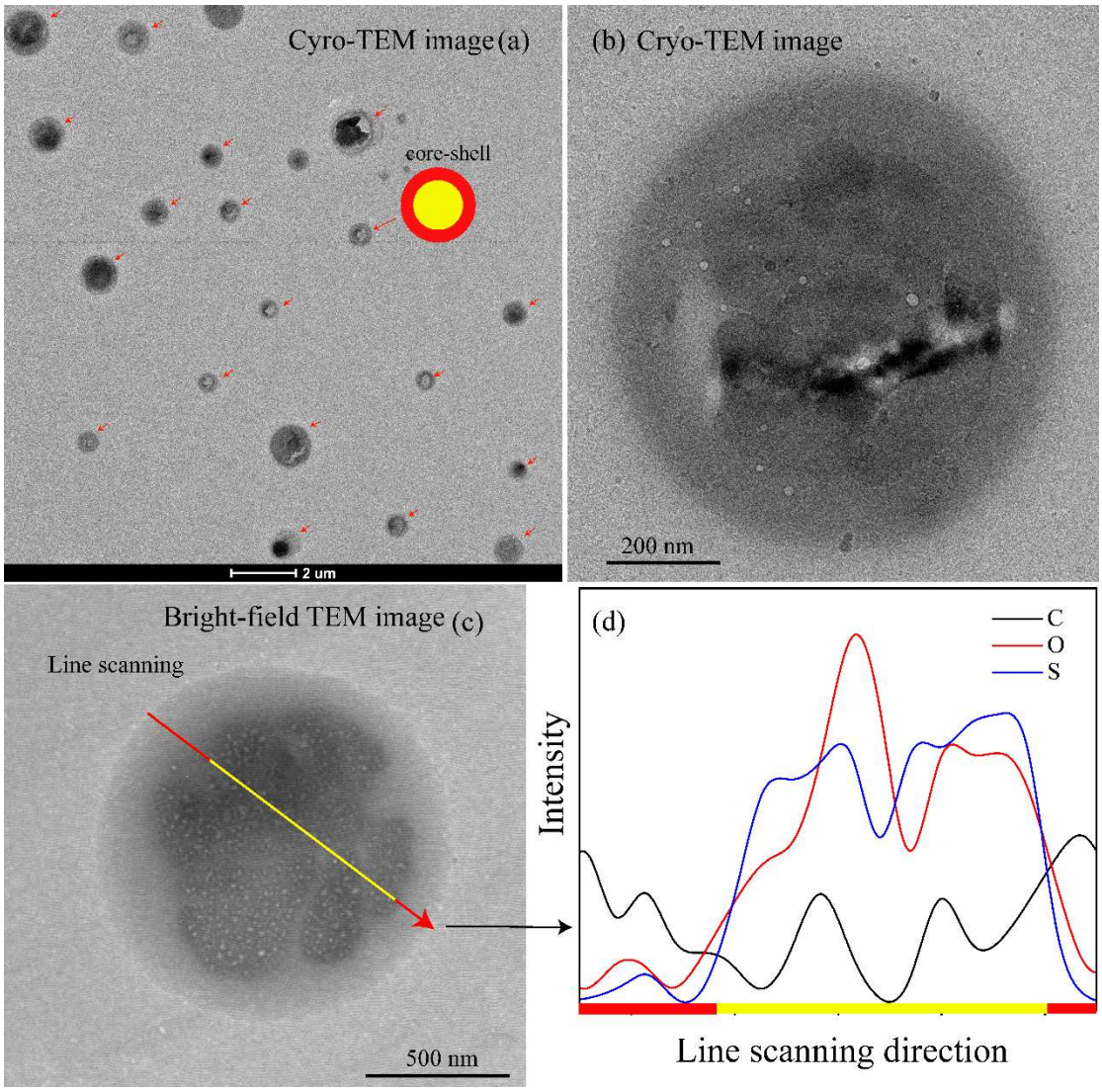

Figure 1 Morphology and composition of secondary particles in the atmosphere. (a) Low magnification cryo-TEM image showing the core-shell structure (i.e., liquid-liquid phase separation) of secondary particles collected at Lesser Khingan Mountain site; (b) High magnification cryo-TEM image showing shell and core; (c-d) A core shell particle and its line scanning in STEM showing C, O, S variations.

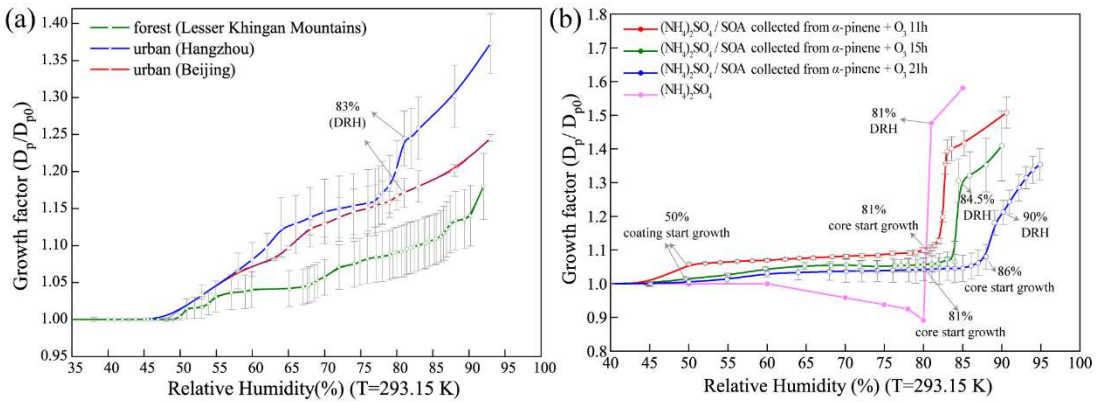

530

531 **Figure 2** Deliquesces and growth factors of ambient particles collected in different

532 environment air (a) and coated $(NH_4)_2SO_4$ particles (after exposing in the

533 photochemical chamber for 11h, 15h, and 21h). The data in Figs. 2a and 2b were

534 obtained from the optical images of the size growth of individual particles under

535 different RHs in Figures 4, S2, and S3.

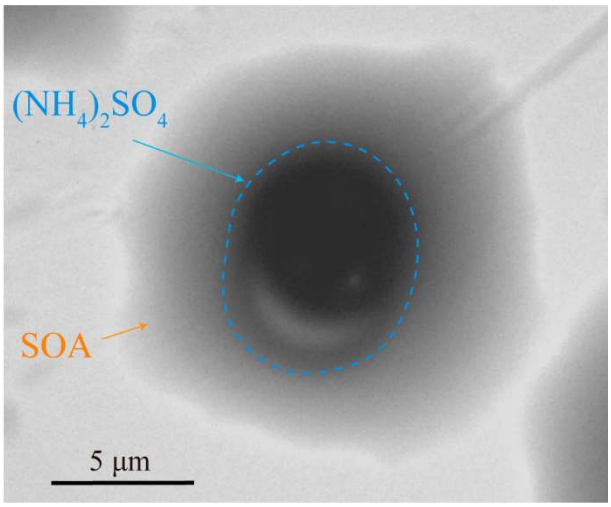

Figure 3 TEM image showing the core-shell shape (i.e., liquid-liquid phase separation) of an individual particle generated from the laboratory flow tube after 21 hrs. The core is the ammonium sulfate and the shell is secondary organic aerosol (SOA).

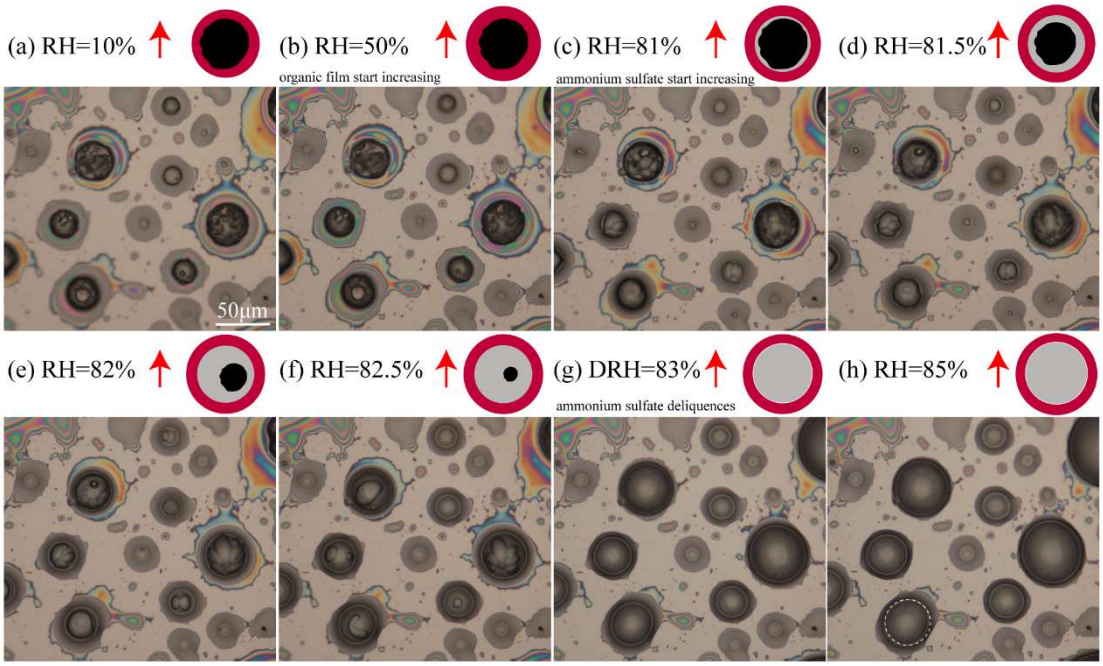

Figure 4 Optical images showing hygroscopic growth during hydration from 5% to 94% RH of individual particles (a-h). The ammonium sulfate particles were coated with organic shell in the flow tube after 11 hours of exposure under different RH at T=293.15 k. Up arrow (↑) represents the RH increase process.